Caribbean Sea eddies inferred from TOPEX/POSEIDON altimetry and a 1/6° Atlantic Ocean model simulation

James A. Carton

and

Yi Chao*

September 24, 1996

To be submitted to the *Journal of Geophysical Research*

Department of Meteorology
University of Maryland
College Park, MD 20742
carton@atmos.umd.edu

*Jet Propulsion Laboratory and California Institute of Technology
Pasadena, CA 91109
yc@pacific.jpl.nasa.gov

Abstract

Large cyclonic and anticyclonic eddies are found in the Caribbean Sea. Analysis of sea level data from the TOPEX/POSEIDON altimeter shows that the eddies are quite regular, appearing once every 80-100 days near the Southern Lesser Antilles. These eddies progress westward at average speeds of 12 cm/s, growing in amplitude up to 20 cm. Many eddies dissipate in the coastal waters of Nicaragua a half-year after they appear. A high resolution general circulation model of the Atlantic is shown to reproduce major features of the eddy life cycle, including their amplitudes, temporal scales, and propagation speed. Analysis of the model output further suggests that the eddies are mainly limited to the thermocline and above with little phase lag in the vertical. The simulated eddies have sufficiently strong currents that the horizontal gradient of total vorticity changes sign, suggesting that conversions from mean to eddy kinetic energy may be contributing to their growth. Analysis of the simulation links eddies in the Caribbean with eddies formed outside the Caribbean at the confluence of the North Brazil Current and North Equatorial Countercurrent systems.

1. Introduction

The Caribbean Sea, a deep semi-enclosed basin, plays an important role in closing the mass budget of the Atlantic Ocean. The mean currents of the Southern Caribbean are dominated by the strong westward Caribbean Current that flows into the basin through the islands of the Southern Lesser Antilles (**Fig. 1**). This current sweeps past the Yucatan Peninsula, and continues into the Gulf of Mexico (Wust, 1964; Gordon, 1967), exiting through the Florida Straits at a rate of 30×10^6 m^3/s (Schmitz and Richardson, 1991). Its speed in the Southern Caribbean may average 60 cm/s (Molinari et al., 1981).

Roughly half of the transport in this current enters the Southern Caribbean through the narrow Grenada, Saint Vincent, and Saint Lucia Passages of the Southern Lesser Antilles (see Mazeika et al., 1983; Kinder et al., 1985 and associated references). Water coming through the Windward Islands is generally assumed to originate in the Southern Hemisphere, transported there by variable currents along the eastern boundary of South America (Schmitz and Richardson, 1991). A few channels are deep enough to admit water to depths of 900m. Other than these narrow channels most of the transport into the Caribbean occurs at depths shallower than 200m. The shallowness of these latter passages ensures that the Caribbean Current has a shallow vertical structure and strong vertical shear in the east.

The Caribbean Sea is also known to have pronounced variability in both space and time. The sea level record at La Guaira in central Venezuela is shown in **Fig. 2**. This port is exposed to the Caribbean Sea with only a 20-kilometer continental shelf. In the time series an annual variation is evident. Weekly timescale variations are apparent, produced by synoptic fluctuations in winds and surface pressure. But, the most energetic signals in the record are quasi-periodic 20 cm peak-to-peak fluctuations with time scales of 80-100 days. We believe the cause of these sea level fluctuations is the westward passing of large amplitude mesoscale eddies. Such eddies are apparent in a hydrographic survey by the Colombian Navy in 1975,

shown in **Fig. 3**. The sources and evolution of these eddies are the main topics of this paper.

The first published evidence of eddy activity in the Southern Caribbean was the discovery of two eddies to the west of the Lesser Antilles by Ingham and Mahnken (1966). These eddies were confined mainly above 150m with maximum surface currents of 1 m/s. In a reexamination of the data, Leming (1971) proposed that the eddies were part of an island wake resulting from flow past the Lesser Antilles. A comprehensive documentation of the eddy field came from deployments of 23 drifters during the fall and winter seasons of 1975-1977 (Molinari et al., 1981; Heburn et al., 1982; Kinder, 1983). The drifter tracks showed evidence of eddy activity throughout the Southern Caribbean. But the distribution of observations led the authors to assume that the eddy activity occurred mainly in the eastern basin. Successive drifters that seemed to measure the same eddy implied westward propagation with speeds of 10 cm/s. Molinari et al. (1981) suggested that the appearance of eddies near the Aves Swell was the result of interaction between the mean flow and the topography. A different generation mechanism was proposed by Heburn et al. (1982) using a two-layer model, suggesting that the eddies result from barotropic instability of the strong currents flowing through the Lesser Antilles.

Because of their sparse distribution, the drifters were unable to resolve the space or time scales of the eddies. Synthetic Aperture Radar measurements from SEASAT (Fu and Holt, 1983) and altimetry from GEOSAT (Nystuen and Andrade, 1993) had both subsequently shown evidence of eddy activity in the Caribbean Sea. Nystuen et al. identified two anticyclonic eddies with 20 cm amplitudes and diameters of 200-300 km. These eddies were much larger and more persistent than those previously described, with a comparable westward speed of 15 cm/s.

In this paper we use sea level information from the TOPEX/POSEIDON satellite altimeters to describe the eddy field in the Caribbean Sea. In addition, an eddy-resolving Atlantic Ocean

general circulation model has recently been developed (Chao et al., 1996). The fine horizontal (1/6°) and vertical (37-level) resolution of this simulation allows us to study aspects of the mesoscale dynamics of the Caribbean Sea that are not visible to surface observations from satellite altimetry or drifters.

2. Altimeter data analysis

Processing of 110 cycles of TOPEX/POSEIDON (T/P) data into sea level records has been carried out by the Geosciences Laboratory/NOAA and is described in detail in Cheney et al. (1994). The equatorial spacing of the orbit, 2.83°, defines the minimum resolved cross-track spatial scales. Orbit precision for the T/P satellite is 5 cm, with most of the error at planetary wavelengths. No filtering has been done to correct for orbit error, as has been necessary with previous altimeter data sets. Ocean tide signals were removed using the tide model of Cartwright and Ray modified by Wagner et al. (1994). The semidiurnal tides are generally weak in the Southern Caribbean (Kjerfve, 1981), and so errors in the semidiurnal tide correction are not expected to be important.

Sea level variability in the Caribbean rises from a root-mean-square 8 cm in the east to 12 cm in the west, decreasing again as one progresses northward (**Fig. 4**). In the western Caribbean seasonal variations are significant, apparently due to the annual fluctuations of the trade winds. Of the 8-12 cm total 2 cm is accounted for by the annual cycle, and most of this is east of 65°W.

The phase of the annual cycle is apparent in the time series shown in **Fig. 5**. In the west sea level is depressed by 10 cm in winter-spring when the trade winds are unusually intense. Sea level is elevated by a similar amount during summer-fall when the trade winds weaken. The amplitude of the annual cycle decreases dramatically west of 70°W.

The time series in **Fig. 5** shows clearly that the increase in sea level variability as one progresses westward into the Caribbean is the result of strong oscillations at intraseasonal periods. To define the time scales of these oscillations we have computed power spectra using the full record length, without any filtering or prewhitening. The results are displayed in a log-linear plot in the lower panel of **Fig. 5**. Most of the intraseasonal energy is in the frequency band between 80-100 days. Within that band inspection of the spectra shows that the dominant time scale increases and the frequency band becomes narrower towards the west. Besides the energy in the 80-100 day band, there is a peak in the spectra with smaller amplitude close to 180 days that may be the semiannual cycle. Unfortunately, the record length is probably too limited to distinguish this clearly from the longest-periods of the intraseasonal variability. At periods of less than 50 days the energy levels drop abruptly. The low energy in this band reduces our concern that high frequency fluctuations are being aliased by the 10-day sampling period of the altimeters.

The strongest variability occurs at 14°N. At this latitude the intraseasonal variability consists mainly of a series of westward propagating eddies whose amplitudes grow as they propagate (**Fig. 6**). The short record length only justifies a simple approach to determining the speed of propagation of the eddies. Here we estimate this speed by measuring the individual speeds of 20 eddies visible in the record. We assume that the statistics are stationary in order to estimate a mean propagation speed, and that the eddy motions are independent and distributed according to a Gaussian distribution to determine an error estimate. Based on these assumptions we obtain an average of 11.7±1 cm/s westward speed. This average is remarkably consistent with the previous estimates of Molinari et al. (1981) and Nystuen and Andrade (1993). We define a zonal scale of the eddies to be the distance from the sea level maximum or minimum to the zero-crossing after the seasonal cycle is removed. According to this procedure the average scale of these eddies is estimated as 250 km. We make no attempt to put confidence limits on this estimate, as it is quite close to the minimum scale resolvable by the

altimeters. It is comforting that the estimate is consistent with that of Nystuen and Andrade (1993), although much larger than earlier drifter studies would suggest.

3. Eddy-resolving Atlantic Ocean model

The ocean model is based on the Parallel Ocean Program (POP) developed at Los Alamos National Laboratory (Dukowicz et al., 1993). This ocean model is based on Bryan's (1969) formulation, but differs from it by removing the rigid-lid approximation and treating the sea surface height as a prognostic variable (i.e., free-surface). The model domain covers the Atlantic ocean from 35°S to 80°N. The horizontal resolution is 1/6° in both longitude and latitude. There are 37 levels in the vertical. For the horizontal subgrid-scale parameterization of tracers and momentum, a highly scale-selective biharmonic (4th order) scheme was used. The conventional second-order operator is used for the vertical subgrid-scale parameterization. The ocean model is closed to inflow and outflow at the open boundaries. To mimic the water exchange processes across these artificial boundaries, "sponge" layers (or "buffer" zones) are introduced next to these closed boundaries at all depths. In these sponge layers temperature and salinity are restored toward the Levitus (1982) seasonal climatology. The width of the sponge layer is about 5°, and the restoring time scale decreases from 30 days for grid points near the prognostic model interior to five days near the boundary.

Starting from Levitus (1982) initial conditions, we have integrated this 1/6° Atlantic Ocean model for a total of twenty-two years. during the first 10 years the model was forced with climatological the wind stress of Hellerman and Rosenstein (1983) and heat flux of Han (1984). Surface salinity was restored to the Levitus (1982) climatology with a timescale of 30 days. During the last 12 years the model was forced with European Center for Medium-Range Weather Forecast (ECMWF) monthly stresses (Trenberth and Olson, 1988; Barnier et al., 1995).

The distribution of simulated sea level variability (**Fig. 7**) is similar to that observed by TOPEX/POSEIDON. Maximum variability is 12 cm at 15°N, decreasing to 8 cm in the east. North of the Yucatan Peninsula the amplitudes are larger than observed, reaching 16 cm. The distribution of energy as a function of frequency also bears strong similarities to the observations (compare **Figs. 5** and **8**). In the east the seasonal cycle is present, although with an amplitude of a few centimeters instead of the 10 centimeters observed. Further west the simulation shows strong variability in the 80-100 day band with a narrow spectral peak exceeding 1×10^4 cm^2s. Energy in periods less than 50 days is greatly reduced at all periods. In the western Caribbean, west of 80°W, the sea level variations are reduced. A time-longitude plot of the simulated sea level is shown in **Fig. 9** at the same latitude, 14°N, as observed sea level was displayed in **Fig. 6**. East of the Caribbean sea level variations are primarily annual. Within the Caribbean eddies grow and propagate westward with an average speed of 12 cm/s, a propagation speed similar to that observed. Spatial scales are also typically 200-300 km.

An instantaneous cross-section of velocity with depth and longitude shows that the eddies are primarily confined to the thermocline with little vertical phase shift (**Fig. 10**), consistent with the observations of Morrison and Nowlin (1982). This latter suggests that baroclinic-type instability processes may play a secondary role. The vertical depth of penetration varies from 200 m near the Lesser Antilles to 800 m near Nicaragua.

4. A case study: the life cycle of an anticyclonic eddy

The life cycle of one anticyclonic eddy is shown in **Fig. 11**. The selection of this particular eddy is purely random. We begin soon after the eddy has been formed in the retroflection of the North Brazil Current (day 7281, **Fig. 11**, upper left). After formation this ring progresses to the northwest at a speed of 15 cm/s until it reaches the Lesser Antilles on day 7371. The details of the circulation at this date are shown in **Fig. 12**. The ring distorts the

inflow into the Caribbean Current, shifting it northward and thus generating a cyclonic circulation to the west of the ring. In the simulation the cyclone- anticyclone pair progresses westward through the Southern Caribbean during an interval of 170 days. During its progression through the Caribbean the amplitude of the eddy doubles. In the simulation these eddies are dissipated further north along the Yucatan Peninsula.

The simulated eddy shedding near the North Brazil retroflection is consistent with recent field observations of Johns et al. (1990) and Fratantoni et al. (1995) showing that the currents along the northeastern margin of Brazil are quasi-periodic with periods between 40-100 days. Based on these observations and images from the Coastal Zone Color Scanner, Johns et al. suggest that the North Brazil retroflection system is unstable, continuously shedding anticyclonic rings. Inspired by this work Richardson et al. (1994) report surface drifter tracks that show two such rings progressing northwestwards to the Lesser Antilles. At that point the eddies either spun-down, or were ejected from the rings. Using the GEOSAT altimeter data Didden and Schott (1993) trace retroflection rings as far as the entrance to the Caribbean Sea, leaving their fate further downstream uncertain.

Fratantoni et al. (1995) revisit the issue of the fate of the rings. They examine a numerical simulation of the tropical Atlantic using a $1/4^{o} \times 1/4^{o}$, six-layer model. Examination of the model output shows that although rings form every 40-60 days, only 2-3 rings per year can be traced to the Lesser Antilles, and none penetrate into the Caribbean. However, in evaluating their model one must consider the complex geometry of the Lesser Antilles. The coastline for that particular model was defined by the 200 m isobath. That approximation and the $1/4^{o}$ resolution effectively close most of the southern passages into the Caribbean in that model (the topography is described in Mazeika et al., 1983 and Kinder et al., 1985).

5. Summary

The sea level observations of the Caribbean are analyzed during the first three years of the TOPEX/POSEIDON altimeter mission. The observations show the presence of large, regular, cyclonic and anticyclonic eddies. These eddies are consistent with earlier sightings of eddies in this area, and with the striking intraseasonal variations in sea level observed at La Guaira, Venezuala. Their presence explains why Gordon (1967) observed counterclockwise circulation in the southwestern Gulf de Los Mosquitos, Molinari et al. (1981) observed clockwise circulation, while Kinder et al. (1985) found counterclockwise circulation had returned.

We use a numerical model simulation, part of an eddy-resolving simulation of Atlantic circulation, to examine several aspects of the dynamics of these eddies. We focus on their origin, ultimate fate, and relationship to the mean circulation of the Caribbean. The conclusions can be summarized as follows:

1) The Caribbean supports strong eddy activity with 80-100 day time scales and 250 km spatial scales. The eddies progress westward with speeds of 12 cm/s, taking approximately 180 days to cross the basin before dissipating near the coast of Nicaragua or the Yucatan Peninsula. The speeds are similar to those of freely propagating waves, but their growth in amplitude westward and changing vertical structure suggests that nonlinear effects are important as well.

2) An eddy-resolving general circulation model of the tropical and North Atlantic has been developed and is found to reproduce these eddies. The simulation results strongly suggest that the eddies ultimately originate in the formation of anticyclonic rings in the North Brazil retroflection. Several data sets show that these rings progress northwestwards toward Port-of-Spain at the entrance to the Southern Caribbean. The simulation presented here extends our understanding of the evolution of these rings by showing them interacting with the topography

associated with the islands of Trinidad and Tobago. The interaction produces a cyclonic circulation to the west of each ring. The resulting pairs of cyclonic and anticyclonic eddies interact with the Caribbean Current and propagate westward along the axis of the Caribbean Current. It appears that the anticyclonic eddies grow significantly as they propagate westward, while the cyclonic eddies eventually decay.

3) The Caribbean Current is the major route by which water enters the Gulf of Mexico, and thus is an important upper branch of the North Atlantic circulation system. The Caribbean Current system has a volume transport of 31×10^6 m^3/s, close to the total transport of the Florida Straits (Gordon, 1967). The eddies may play an important role in mixing thermocline water masses of the Southern and Northern Hemispheres.

Our hypothesis of the generating mechanism of the Caribbean Sea eddies must be treated as tentative. The numerical ocean model used in this study has not been integrated for a sufficiently long time yet for an equilibrium solution, mainly because of the computational cost. Further sensitivity experiments are required to confirm our eddy generation hypothesis. More in-depth analysis of the present simulation still remains to be done to understand the dynamical processes associated with these Caribbean eddies.

Acknowledgements

The authors thank F. Muller-Karger for providing the sea level time series at La Guaira, Venezuala and to R.E. Cheney and the Geosciences Laboratory/NOAA for providing the altimetry. The numerical simulation described in this publication was carried out by YC at the Jet Propulsion Laboratory (JPL), California Institute of Technology, under a contract with National Aeronautics and Space Administration. Computations were performed on the 256-processor Cray T3D massively parallel computer through the JPL Supercomputing Project. JAC has been supported by the National Science Foundation under Grant OCE9416894.

References

Barnier, B., L. Siefridt, and P. Marchesiello, 1995: Thermal forcing for a global ocean circulation model from a three-year climatology of ECMWF analysis, *J. Mar. Sys.*, **6**, 363-380.

Bryan, K., 1969: A numerical method for the study of the circulation of the world ocean, *J. Comp. Phys.*, **4**, 1687-1712.

Centro Colombiano de Datos Oceanograficos, 1983: Crucero Oceano IV - Areas 2 and 3, Republica de Columbia Armada Nacional, 8pp., 9 tables, 43 figures.

Chao, Y., A Gangopadhyay, F. Bryan, and W.R. Holland, 1996: Modeling the Gulf Stream System: how far from reality?, *Geophys. Res. Letts.*, ~~submitted.~~ in press

Cheney, R., L. Miller, R. Agreen, N. Doyle, and J. Lillibridge, 1994: TOPEX/POSEIDON: the 2-cm solution, *J. Geophys. Res.*, **99**, 1,150- 1,165.

Didden, N. and F. Schott, 1993: Eddies in the North Brazil Current retroflection region observed by GEOSAT altimetry, *J. Geophys. Res.*, **98**, 20,121-20,131.

Dukowicz, J.K., R.D. Smith, and R.C. Malone, 1993: A Reformulation and Implementation of the Bryan-Cox-Semtner Ocean Model on the Connection Machine, *J. Atmos. and Oceanic Tech.*, **10**, 195-208.

Fratantoni, D.M., W.E. Johns, and T.L. Townsend, 1995: Rings of the North Brazil Current: their structure and behavior inferred from observations and a numerical simulation, *J. Geophys. Res.*, **100**, 10,633-10,654.

Fu, L.L. and B. Holt, 1983: Some examples of oceanic mesoscale eddies by the SEASAT synthetic-aperture radar, *J. Geophys. Res.*, **88**, 1844-1852.

Gordon, A.L., 1967: Circulation in the Caribbean Sea, *J. Geophys. Res.*, **72**, 6207-6223.

Han, Y.J., 1984: A numerical world ocean General Circulation Model, Part II: a baroclinic experiment, *Dyn. Atmos. Ocean*, **8**,141-172.

Heburn, G.W., T.H. Kinder, J.H. Allender, and H. E. Hurlburt, 1982: A numerical model of eddy generation in the southeastern Caribbean Sea, in *Hydrodynamics of Semi-enclosed Seas*, J.C.J. Nihoul, editor, Elsevier, New York. 555pp.

Hellerman, S., and M.J. Rosenstein, 1983: Normal monthly windstress over the world ocean with error estimates, *J. Phys. Oceanogr.*, **13**, 1093-1104.

Ingham, M.C., and C.V.W. Mahnken, 1966: Turbulence and productivity near St. Vincent Island, B.W.I. A preliminary report, *Carib. J. Sci.*, **6**, 83-87.

Johns, W.E., T.N. Lee, and F.A. Schott, 1990: The North Brazil Current retroflection: seasonal structure and eddy variability, *J. Geophys. Res.*, **95**,22,103-22,120.

Kinder, T., 1983: Shallow currents in the Caribbean Sea and Gulf of Mexico as observed with satellite-tracked drifters, *Bull. Marine Sci.*, **33**, 239-246.

Kinder, T.H., G.W. Heburn, and A.W. Green, 1985: Some aspects of the Caribbean circulation, *Marine Geol.*, **68**, 25-52.

Kjerfve, B, 1981: Tides in the Caribbean Sea, *J. Geophys. Res.*, **86**, 4,243-4,247.

Leming, T.D., 1971: Eddies west of the southern Lesser Antilles In: *Symposium on Investigations and Resources of the Caribbean Sea and Adjacent Regions*, UNESCO, Paris. pp.113-120.

Levitus, S., 1982: Climatological Atlas of the world ocean, NOAA Professional Paper 13, U.S. Department of Commerce, Rockville, MD, 174pp.

Mazeika, P.A., T.H. Kinder, and D.A. Burns, 1983: Measurements of subtidal flow in the Lesser Antilles passages, *J. Geophys. Res.*, **88**, 4483-4488.

Molinari, R.L., M. Spillane, I. Brooks, D. Atwood, and C. Duckett, 1981: surface currents in the Caribbean Sea as deduced from lagrangian observations, *J. Geophys. Res.*, **86**, 6,537-6,542.

Morrison, J.M., and W.D. Nowlin, Jr., 1982: General distributions of water masses within the

eastern Caribbean Sea during the winter of 1972 and the fall of 1983, *J. Geophys. Res.*, **87**, 4,207-4,229.

Muller-Karger, F.E., and R.A. Castro, 1994: Mesoscale processes affecting phytoplankton abundance in the southern Caribbean Sea, *Cont. Shelf Res.*, **14**, 199-221.

Nystuen, J.A., and C.A. Andrade, 1993: Tracking mesoscale ocean features in the Caribbean Sea using Geosat altimetry, *J. Geophys. Res.*, **98**, 8,389-8,394.

Richardson, P.L., G.E. Hufford, R. Limeburner, and W.S. Brown, 1994: North Brazil current eddies, *J. Geophys. Res.*, **99**, 5,081-5,093.

Schmitz, W.J. Jr., and P.L. Richardson, 1991: On the sources of the Florida Current, . Deep-Sea Res., **B38**, suppl. 1, S379-S409.

Trenberth, K.E., and J.G. Olson, 1988: ECMWF global analysis 1979-86: circulation statistics and data evaluation, NCAR Tech. Note, NCAR/TN-300+STR, 94pp, 12 fiche.

Wagner, C.A., C.K. Tai, and J.M. Kuhn, 1994: Improved M2 ocean tide from TOPEX/POSEIDON and Geosat altimetry, *J. Geophys. Res.*, **99**, 24,853-24,866.

Wust, G., 1964: Stratification and circulation in the Antillean-Caribbean Basin. Columbia University Press, New York, 201pp.

Figure Legends

Fig. 1 Basin geometry. Dashed line shows 1000 meter isobath. Instantaneous path of the Caribbean Current is sketched.

Fig. 2 Daily sea level at La Guaira, Venezuala (10.60°N, 66.94°W) for three years. Data have been daily-averaged (data are described in Muller-Karger and Castro, 1994). Lower panel shows spectrum.

Fig. 3 Temperature at 100 m depth based on observations collected by the Colombian Navy between June 24 and July 23, 1975 (Centro Colombiano de Datos Oceanograficos, 1983).

During the month-long cruise the research vessel *San Andres* collected 63 stations, beginning in the west and progressing eastward (indicated by dots). The eddies are spaced approximately 3° apart.

Fig. 4 Observed root-mean-square sea surface height. Contour interval is 2 cm.

Fig. 5 Observed sea level at four longitudes along 14°N. Upper panel shows time series, lower panel shows power spectra.

Fig. 6 Cross-section of observed sea level with longitude and time at 14°N. Contour interval is 5 cm.

Fig. 7 Simulated root-mean-square sea level. Contour interval is 2 cm.

Fig. 8 Simulated sea level at four longitudes along 14°N. Upper panel shows time series, lower panel shows power spectrum.

Fig. 9 Cross-section of simulated sea level with longitude and time at 14°N. Contour interval is 5 cm.

Fig. 10 Vertical structure of simulated temperature, salinity, and velocity at 14°N on day 6780.

Fig. 11 Model simulation sea level height at 30-day intervals. Note the penetration of an anti-cyclonic eddy into the Caribbean Sea.

Fig. 12 Details of simulated SST and surface current speed for one day, 7371, shown in **Fig. 11**. Region is 5°N–15°N, 70°W–50°W.

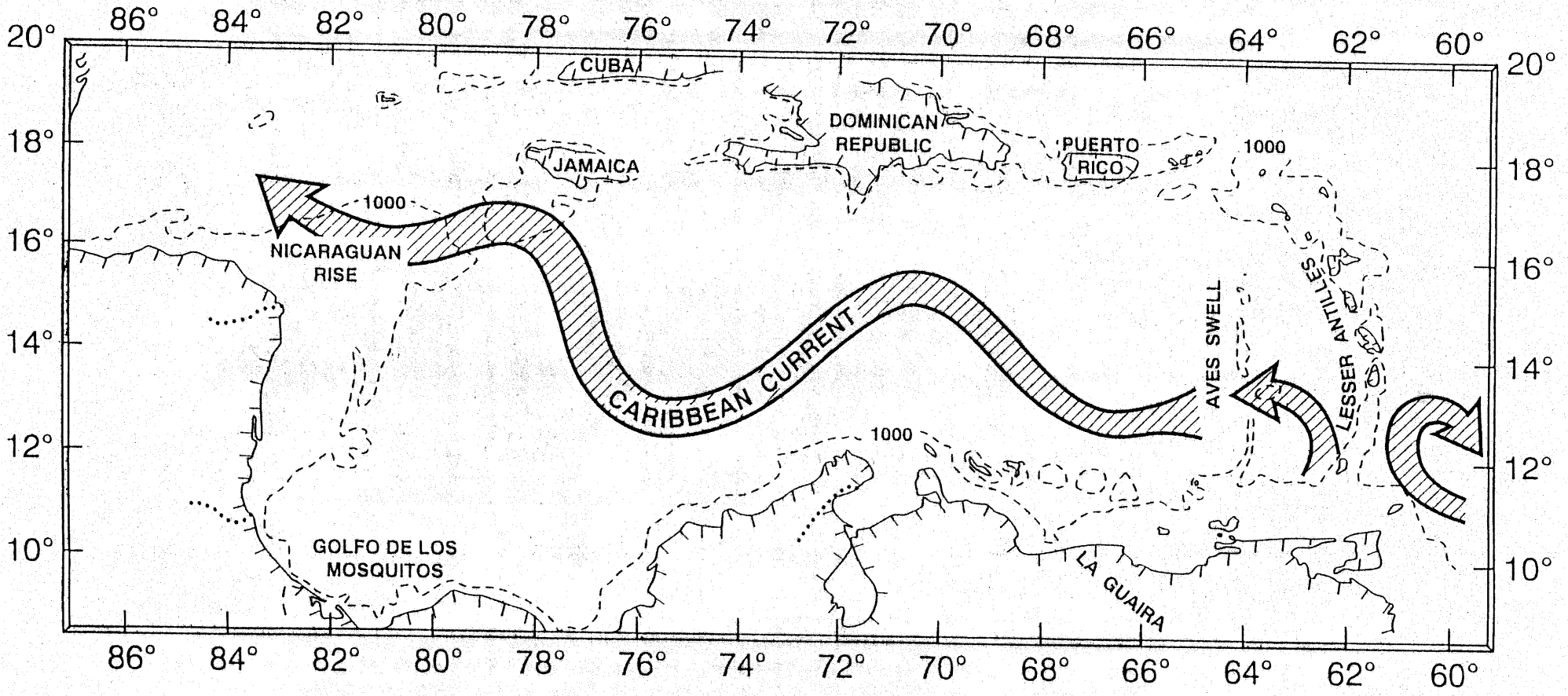
86° 84° 82° 80° 78° 76° 74° 72° 70° 68° 66° 64° 62° 60°
20° 18° 16° 14° 12° 10°
CUBA
JAMAICA
DOMINICAN REPUBLIC
PUERTO RICO
1000
NICARAGUAN RISE
CARIBBEAN CURRENT
AVES SWELL
LESSER ANTILLES
GOLFO DE LOS MOSQUITOS
LA GUAIRA

Fig. 1

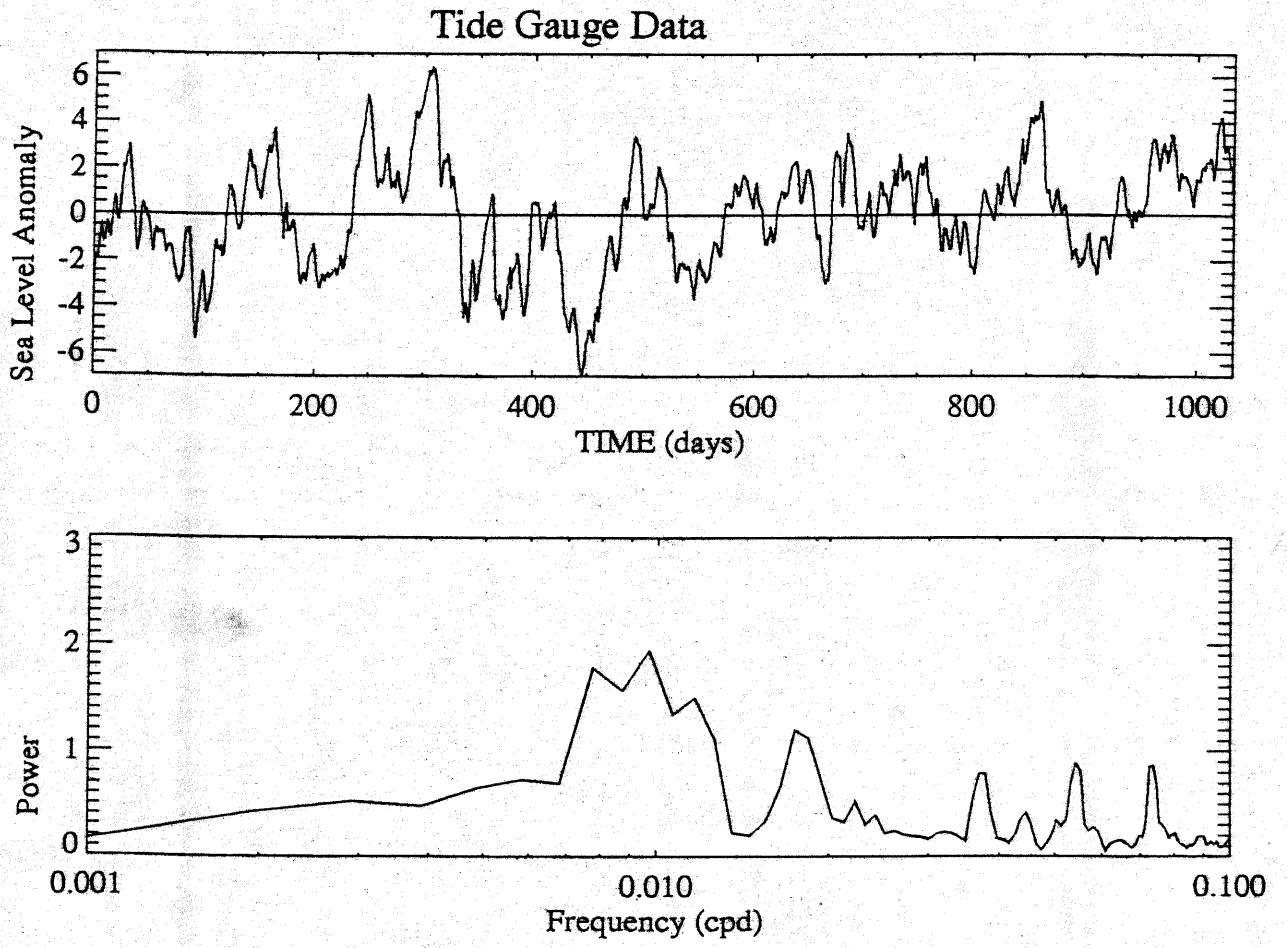
Tide Gauge Data
Sea Level Anomaly
6
4
2
0
-2
-4
-6
0
200
400
600
800
1000
TIME (days)
Power
3
2
1
0
0.001
0.010
0.100
Frequency (cpd)

Fig. 2

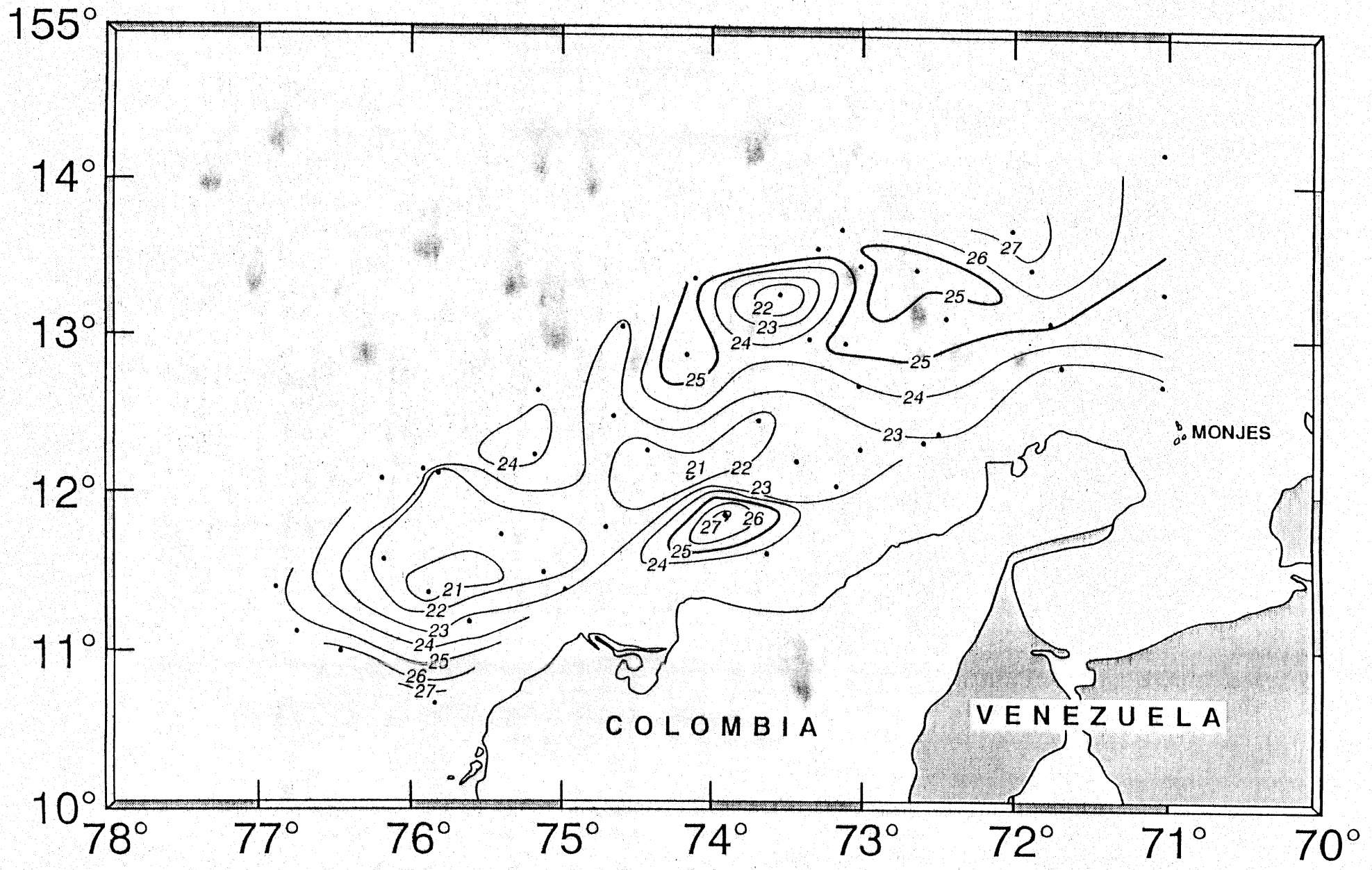
155°
14°
13°
12°
11°
10°
78°
77°
76°
75°
74°
73°
72°
71°
70°
COLOMBIA
VENEZUELA
MONJES
21
22
23
24
25
26
27

Fig. 3

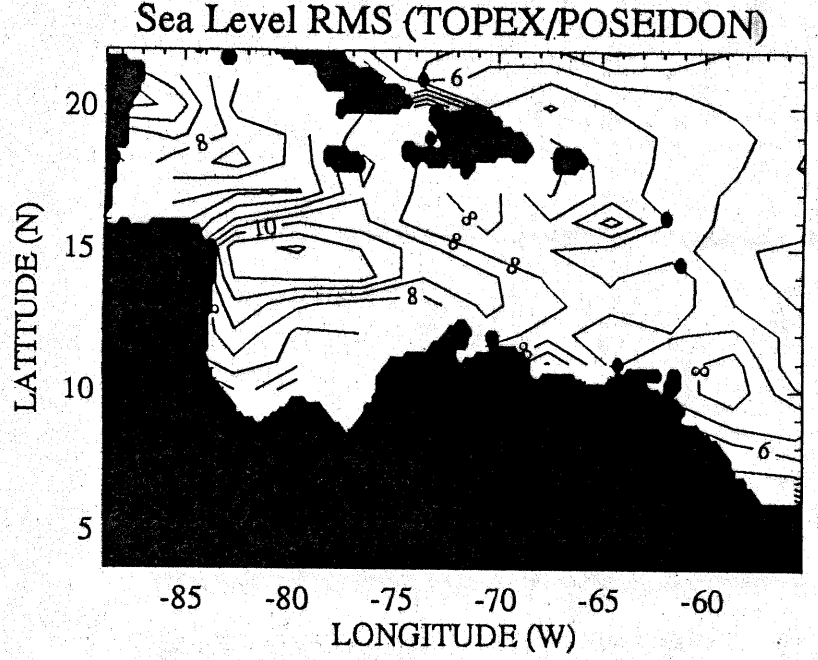
Sea Level RMS (TOPEX/POSEIDON)
LATITUDE (N)
20
15
10
5
-85
-80
-75
-70
-65
-60
LONGITUDE (W)
6
8
10
8
8
8
8
8
8
6

Fig. 4

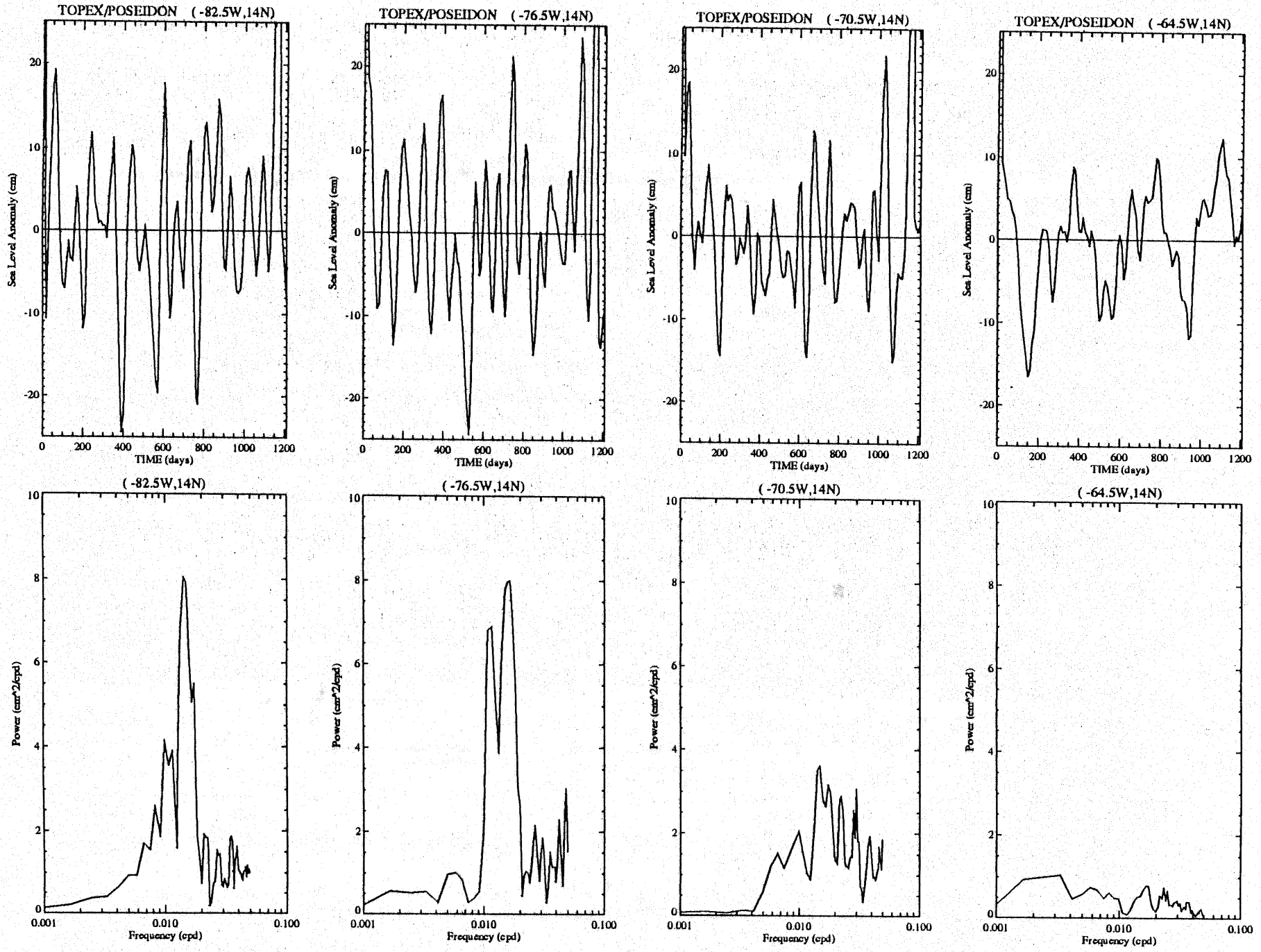
TOPEX/POSEIDON (-82.5W,14N)
TOPEX/POSEIDON (-76.5W,14N)
TOPEX/POSEIDON (-70.5W,14N)
TOPEX/POSEIDON (-64.5W,14N)
Sea Level Anomaly (cm)
TIME (days)
(-82.5W,14N)
(-76.5W,14N)
(-70.5W,14N)
(-64.5W,14N)
Power (cm^2/cpd)
Frequency (cpd)

Fig 5

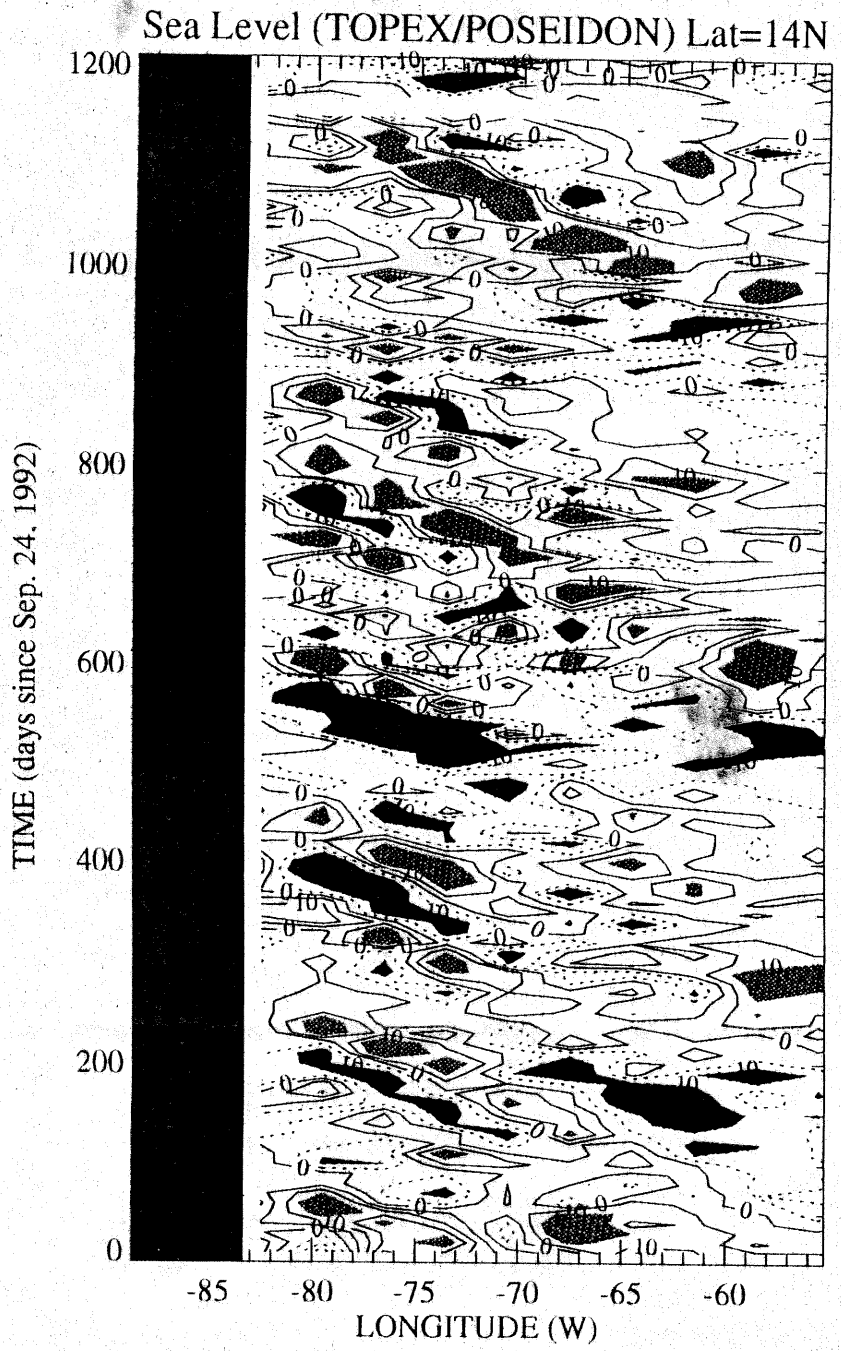
Sea Level (TOPEX/POSEIDON) Lat=14N
TIME (days since Sep. 24, 1992)
1200
1000
800
600
400
200
0
-85
-80
-75
-70
-65
-60
LONGITUDE (W)

Fig. 6

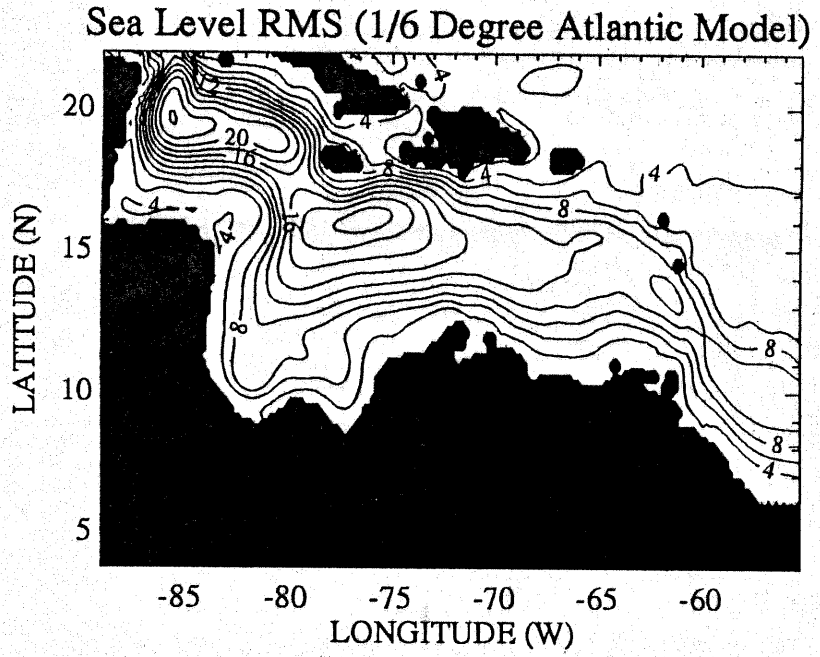
Sea Level RMS (1/6 Degree Atlantic Model)
LATITUDE (N)
20
15
10
5
-85
-80
-75
-70
-65
-60
LONGITUDE (W)

Fig. 7

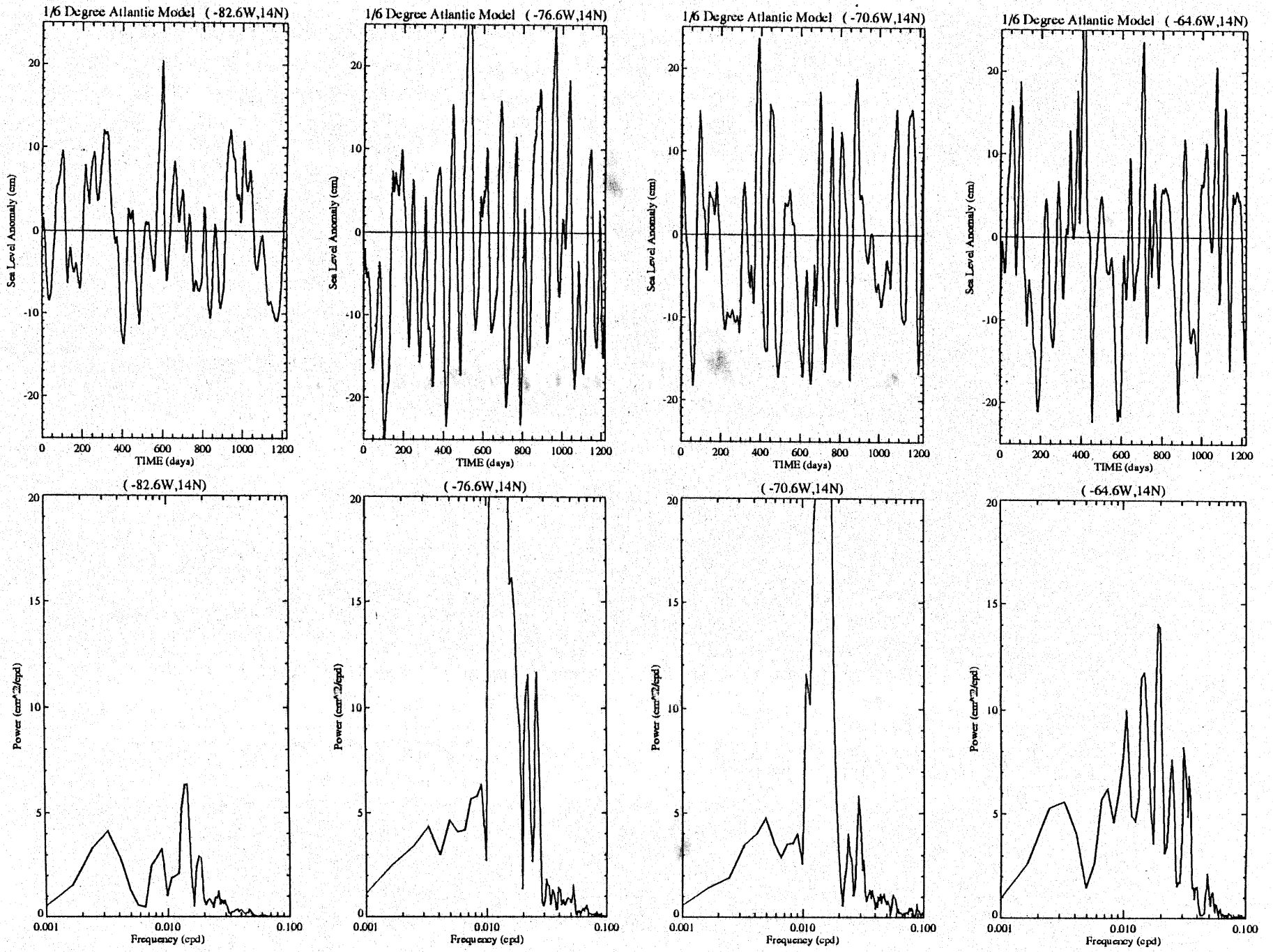
1/6 Degree Atlantic Model (-82.6W,14N)
1/6 Degree Atlantic Model (-76.6W,14N)
1/6 Degree Atlantic Model (-70.6W,14N)
1/6 Degree Atlantic Model (-64.6W,14N)
Sea Level Anomaly (cm)
TIME (days)
(-82.6W,14N)
(-76.6W,14N)
(-70.6W,14N)
(-64.6W,14N)
Power (cm^2/cpd)
Frequency (cpd)

Fig. 8

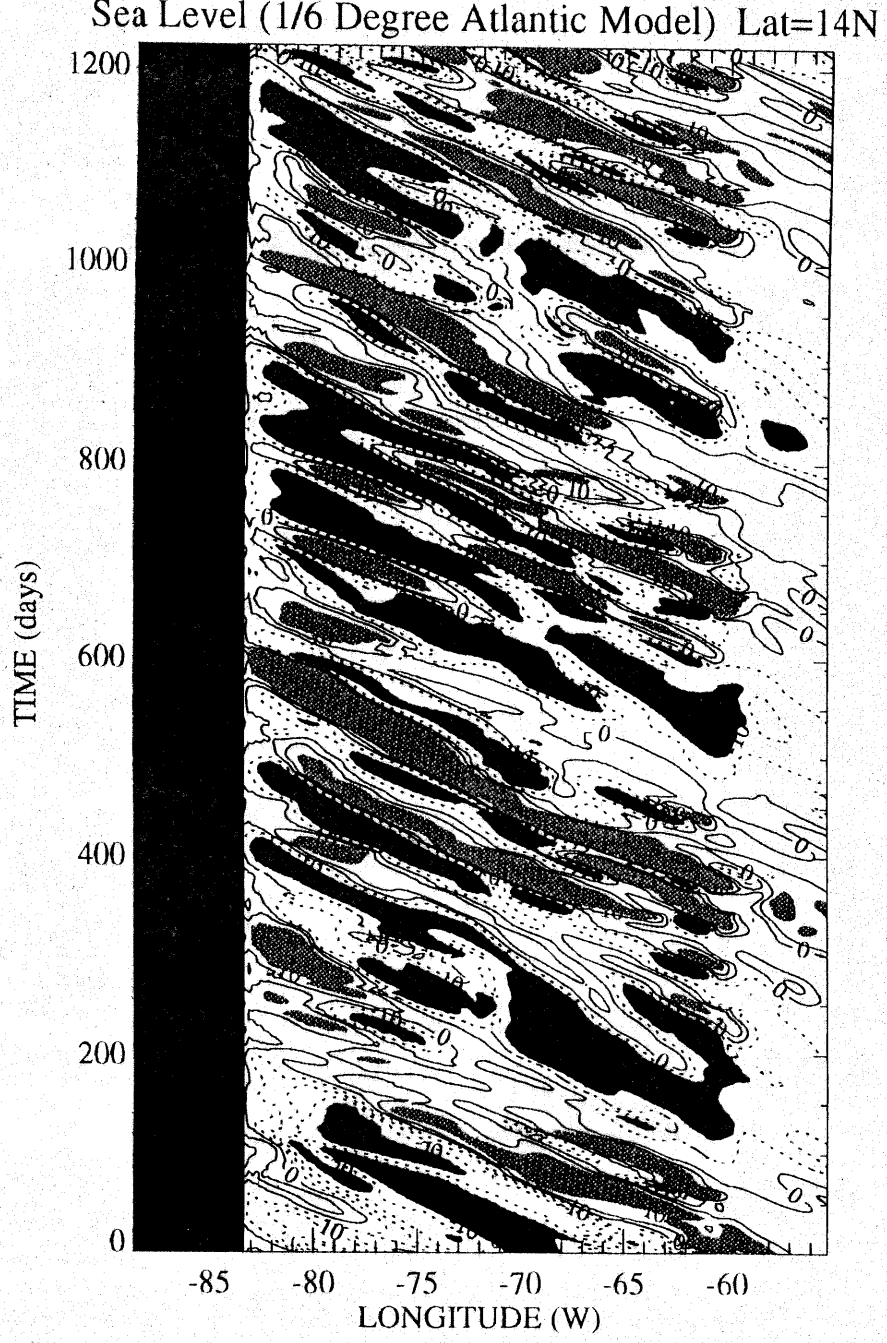
Sea Level (1/6 Degree Atlantic Model) Lat=14N
TIME (days)
1200
1000
800
600
400
200
0
-85
-80
-75
-70
-65
-60
LONGITUDE (W)

Fig. 9

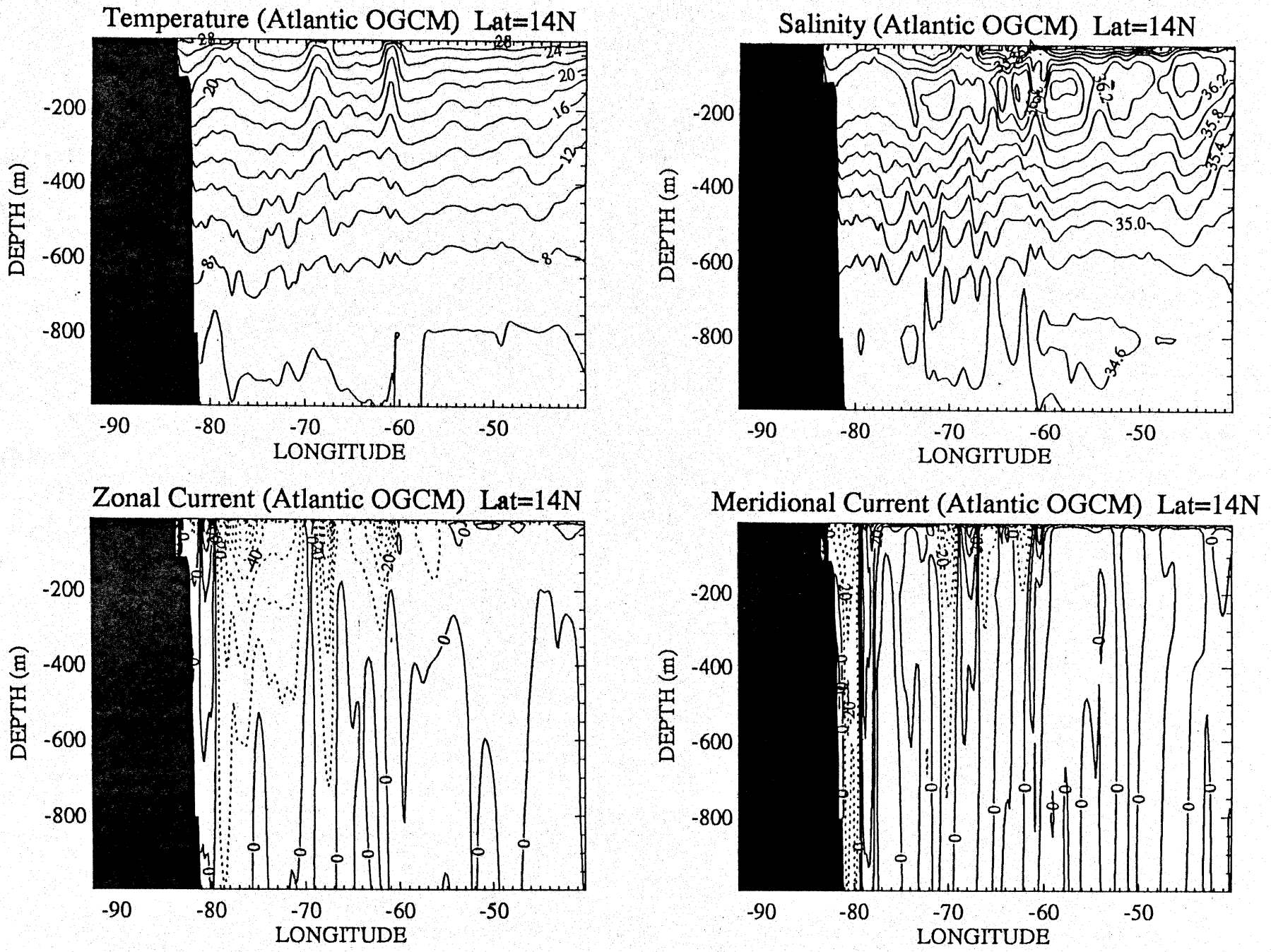
Temperature (Atlantic OGCM) Lat=14N
Salinity (Atlantic OGCM) Lat=14N
Zonal Current (Atlantic OGCM) Lat=14N
Meridional Current (Atlantic OGCM) Lat=14N
DEPTH (m)
-200
-400
-600
-800
-90
-80
-70
-60
-50
LONGITUDE

Fig. 10

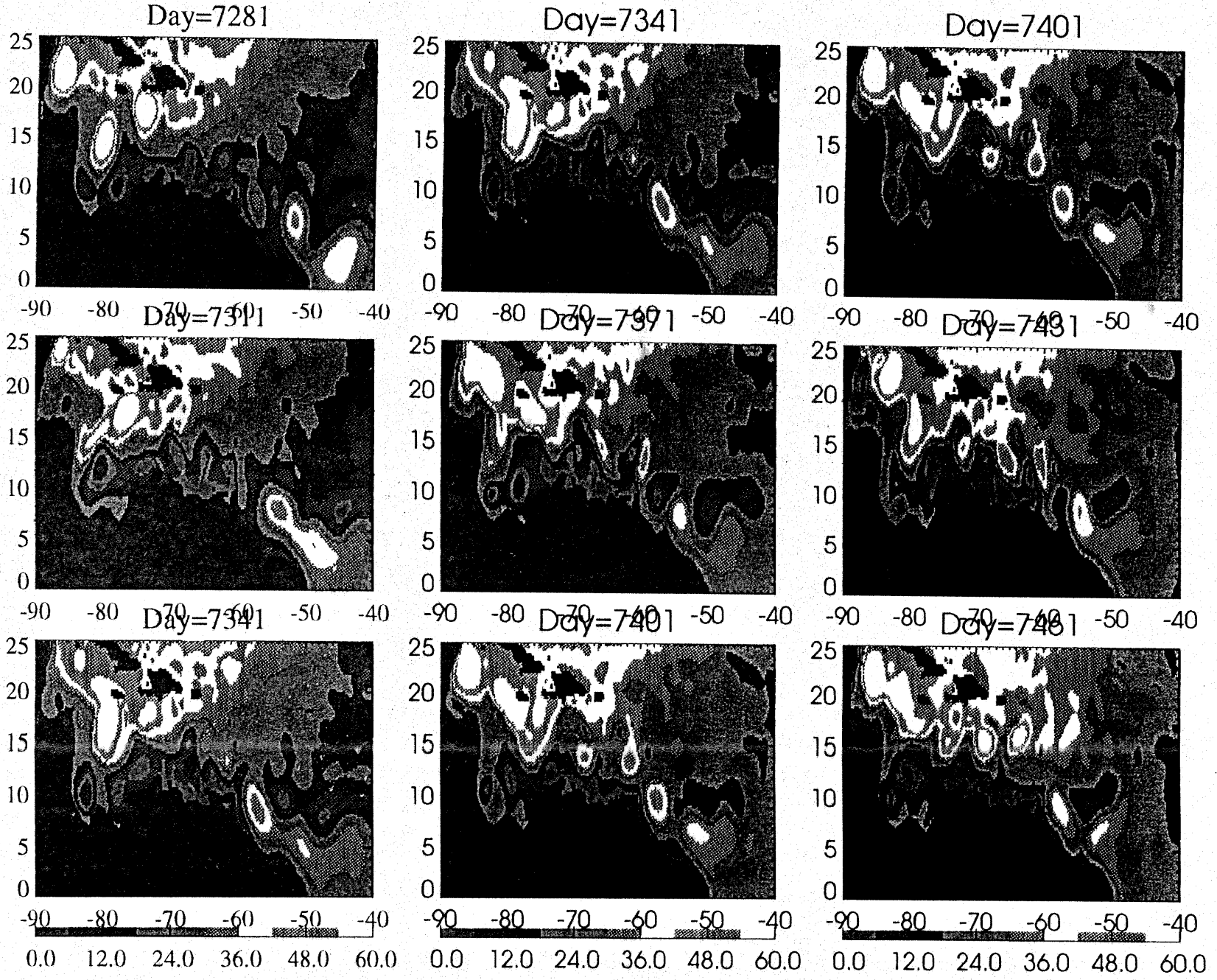
Day=7281
Day=7341
Day=7401
Day=7311
Day=7371
Day=7431
Day=7341
Day=7401
Day=7461
25
20
15
10
5
0
-90 -80 -70 -60 -50 -40
0.0 12.0 24.0 36.0 48.0 60.0

Fig. 11

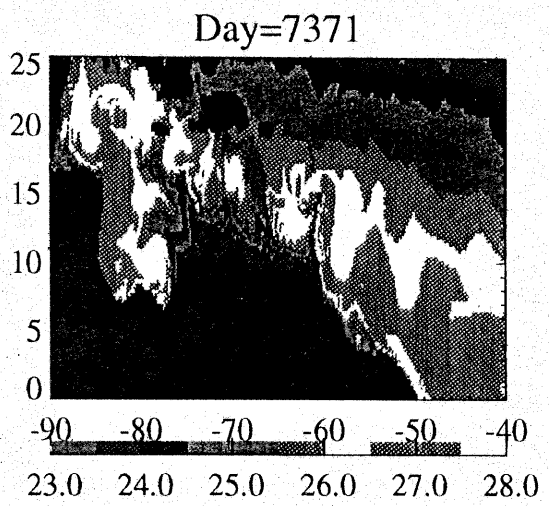

Fig 12a

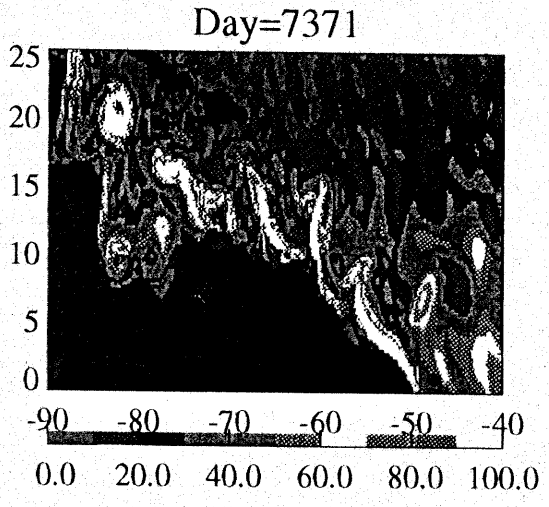

Fig 12b